ROYAL SOCIETY OF CHEMISTRY

EDGE ARTICLE

Check for updates

Intramolecular donor-stabilized tetra-coordinated germanium(IV) di-cations and their Lewis acidic properties†

Balakrishna Peddi,[a] Souvik Khan,[a] Rajesh G. Gonnade, [b] Cem B. Yildiz [*c] and Moumita Majumdar [*a]

We report the first examples of intramolecular phosphine-stabilized tetra-coordinated germanium(IV) di-cationic compounds: $[L^{iPr}_2Ge][CF_3SO_3]_2$ **3^{iPr}** and $[L^{Ph}_2Ge][CF_3SO_3]_2$ **3^{Ph}** (L^{iPr} = 6-(diisopropylphosphanyl)-1,2-dihydroacenaphthylene-5-ide; L^{Ph} = 6-(diphenylphosphanyl)-1,2-dihydroacenaphthylene-5-ide). The step wise synthetic strategy involves the isolation of neutral and mono-cationic Ge(IV) precursors: $[L^{iPr}_2GeCl][X]$ (X = GeCl₃ **1^{iPr}**, OTf **2^{iPr}**), $[L^{Ph}_2GeCl_2]$ **1^{Ph}** and $[L^{Ph}_2GeCl][OTf]$ **2^{Ph}**. Both **3^{iPr}** and **3^{Ph}** exhibit constrained spiro-geometry. DFT studies reveal the dispersion of di-cationic charges over P–Ge–P sites. Anion or Lewis base binding occurs at the Ge site resulting in relaxed distorted trigonal bipyramidal/ tetrahedral geometry. **3^{iPr}** and **3^{Ph}** activate the Si–H bond initially at the P-site. The hydride ultimately migrates to the Ge-site rapidly giving $[L^{Ph}_2GeH][CF_3SO_3]$ **3^{Ph}H**, while sluggishly forming $[L^{iPr}_2GeH][CF_3SO_3]$ **3^{iPr}H**. Compounds **3^{iPr}** and **3^{Ph}** were tested as catalysts for the hydrosilylation of aromatic aldehydes. While catalytic hydrosilylation proceeded via the initial Et₃Si−H bond activation in the case of **3^{iPr}**, compound **3^{Ph}** as a catalyst showed a masked Frustrated Lewis Pair (FLP) type reactivity in the catalytic cycle.

Introduction

Germanium(II) di-cations stabilized by neutral Lewis bases have been known for long,[1] possessing inherent electrophilicity[2] and rarely exhibiting nucleophilic behaviour.[3] In contrast there are only very few examples of Ge(IV) di-cations known, which are stabilized by hyper-coordination involving neutral donors: $[LGeF_2]^{2+}$ (L = tris(1-ethyl-benzoimidazol-2-ylmethyl)amine) (Fig. 1A),[4] $[GeF_2(OTf)_2]$ (OTf = CF₃SO₃) coordinated by two mono-dentate phosphine donors or bi-dentate chelating phosphine donors (Fig. 1B),[5] and $[Me_2Ge(OTf)_2]$ coordinated by two 4-N,N′-dimethylaminopyridine (DMAP) units or a 2,2′-bipyridine (Fig. 1C).[6] Alongside in silicon chemistry, terpyridine-stabilized silicon(IV) di-cations (R_2Si^{2+}), tri-cations (RSi^{3+}),[7] and silicon tetrakis(trifluoromethanesulfonate)[8] have been established as

Lewis superacids[9] in recent times. The uses of Ge(IV) di-cations as Lewis acids hold immense potential; however they are yet to be unfolded. In general, while scheming Lewis acidic Ge(IV) polycations, an optimal balance between the stabilization of the polycationic species by neutral donors and accessibility of vacant orbitals is necessary. Therefore, focused investigations on the stabilization of Ge(IV) polycations using suitable donor groups that circumvent hyper-coordination are imperative for their potential Lewis acidity. Furthermore, isolation of such species has remained a worthwhile synthetic target on fundamental grounds.

As a matter of fact, compared to silicon analogues,[10] there are scarce reports on Ge-based Lewis acids[11] both in their neutral or cationic forms. Greb *et al.* have pioneered neutral bis(perchlorocatecholato)germane as both hard and soft Lewis superacids (Fig. 1D).[12] Bis(catecholato)germane derivatives have been successfully implemented as Lewis acid catalysts.[13] A significant example of the cationic form of Ge(IV) Lewis acid is [(TPFC)Ge(THF)₂]⁺ (TPFC = tris(pentafluorophenyl)corrole, THF = tetrahydrofuran) (Fig. 1E).[14] Recently, a Ge(II) mono-cationic σ-donor ligand towards Ni(0) has been reported with simultaneous Lewis superacidity.[15] It is worth mentioning that Gabbaï *et al.* have demonstrated a formally cationic Ge(IV) σ-acceptor site in a dinuclear Pt–Ge(IV) complex.[16]

Contemporary research in the field of main-group Lewis acids[17] has introduced the concepts of geometrically constrained Lewis acids,[18] main group Lewis acid/ligand assisted

ᵃDepartment of Chemistry, Indian Institute of Science Education and Research, Pune, Dr. Homi Bhabha Road, Pashan, Pune-411008, Maharashtra, India. E-mail: moumitam@iiserpune.ac.in

ᵇPhysical and Materials Chemistry Division, CSIR-National Chemical Laboratory, Pune-411008, Maharashtra, India

ᶜDepartment of Aromatic and Medicinal Plants, Aksaray University, 68100 Aksaray, Türkiye
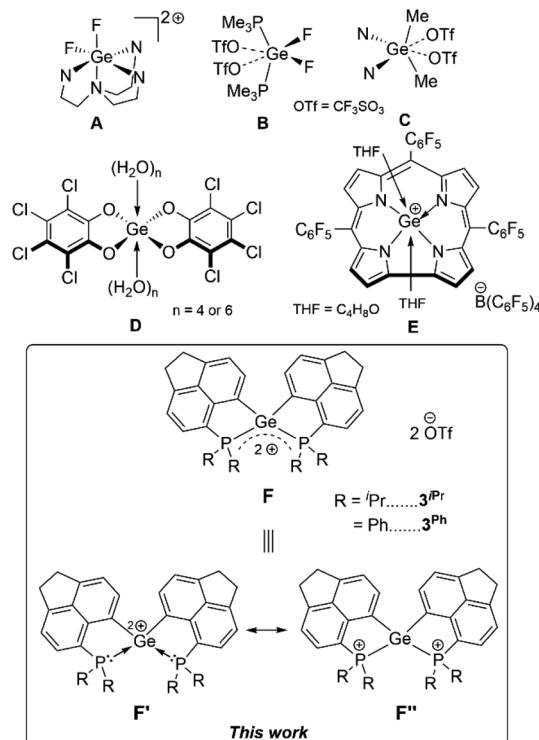
Fig. 1 Reported examples of Ge(IV) di-cations (A) (N4 = tris(1-ethyl-benzoimidazol-2-ylmethyl)amine) and (B) and (C) (N = 4-N,N′-dimethylaminopyridine); examples of Ge(IV)-based Lewis acids (D) and (E) and the intramolecular phosphine-stabilized Ge(IV) di-cations (F, this work).

cooperative bond activation,[19] hidden frustrated Lewis pair (FLP) chemistry[20] in intra-molecular Lewis base stabilized Lewis acidic fragments.[21] Taking advantage of the enforced proximity

in peri-substituted acenaphthenes,[22] herein we have established the unprecedented intramolecularly phosphine-stabilized tetra-coordinated di-cationic Ge(IV) compounds. The aptitude of these geometrically constrained Ge(IV) di-cationic species as Lewis acids has been assessed based on experimental findings and computational analyses. Non-innocent roles of the phosphines have been observed. The proclivity of Ge(IV) di-cationic compounds for $Et_3Si–H$ bond activation coupled with FLP-type reactivity has been realized in a proof-of-concept catalytic hydrosilylation of p-methyl benzaldehyde.

Results and discussion

Syntheses and characterization of intramolecular phosphine-stabilized Ge(IV) mono- and di-cationic compounds

Intramolecular phosphine-stabilized Ge(IV) di-cationic compounds 3^{iPr} and 3^{Ph} were obtained in a step-wise manner as shown in Scheme 1. Initially, L^{iPr}–Br and L^{Ph}–Br were synthesized and characterized (see the ESI† for Experimental procedures). Table 1 summarizes the NMR data for all compounds. The reaction between 1.5 equivalents of lithiated L^{iPr}–Br and $GeCl_4$ at −78 °C in a tetrahydrofuran (THF) medium, followed by extraction with dichloromethane (DCM), gave 1^{iPr} (Scheme 1a). Structural elucidation of the single crystals of 1^{iPr} obtained from acetonitrile (MeCN) reveals the formation of $[L^{iPr}_2GeCl]^+$, interestingly possessing $GeCl_3$ as a counter anion (Fig. S95, ESI†). The formation of the $GeCl_3$ anion stems from the reducing ability of phosphines.[23] The mono-cationic compound 1^{iPr} was characterized by the $^{31}P\{^1H\}$ NMR chemical shift at −11.1 ppm. An additional peak at −19.5 ppm was observed in the $^{31}P\{^1H\}$ NMR spectrum of the crude reaction mixture arising from the corresponding P(V) oxidized product (Fig. S7, ESI†).[24] Using straightforward
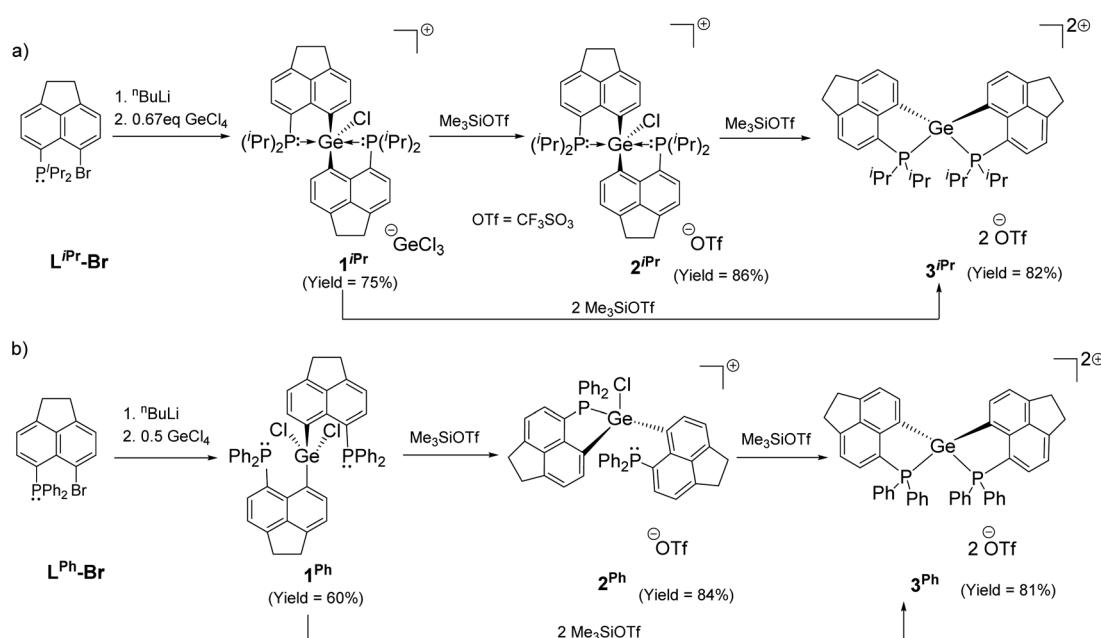
Scheme 1 Syntheses of the Ge(IV) mono- and di-cationic compounds (see the ESI† for the detailed spectroscopic and experimental procedures of each reaction).

Table 1 NMR data for all compounds

Compounds	^{31}P{^{1}H} in ppm (deuterated solvent)	^{19}F{^{1}H} in ppm (deuterated solvent)	J values (Hz)	Compounds	^{31}P{^{1}H} in ppm (deuterated solvent)	^{19}F{^{1}H} in ppm (deuterated solvent)	J values (Hz)
L^{iPr}Br	−1.58^a (CDCl$_3$)			**3^{iPr}DMAP**^{c}	+28.37 (**3^{iPr}**), −13.19 (P^{i}Pr$_2$)^b (CD$_2$Cl$_2$)		
L^{Ph}Br	−9.40^a (CDCl$_3$)			**3^{Ph}(DMAP)$_2$**	−29.16^b (CDCl$_3$)	−79.21^a (CDCl$_3$)	
1^{iPr}	−11.06^a (CDCl$_3$)			**3$^{iPr}_F$**	−10.23(d)^a (CDCl$_3$)	−78.12(OTf), −141.03(t)^a (CDCl$_3$)	$^2J_{P–F}$ = 184.9
1^{Ph}	−34.79^a (CDCl$_3$)			**3$^{Ph}_F$**^{c}	−17.54(br.)^a, −10.27(m), −23.66(m) (CDCl$_3$)	−150.32(t)^a (CDCl$_3$)	$^2J_{P–F}$ = 100.6^a, $J_{P–P}$ = 119.8, $J_{P–F}$ = 98.9^b
2^{iPr}	−10.77^a (CDCl$_3$)	−78.08^a (CDCl$_3$)		**3^{Ph} + Ph$_3$CCl**^{c}	−6.31(**3^{Ph}**), −13.46(**2^{Ph}**)^a (CDCl$_3$)		
2^{Ph}	−13.20^a, −3.0(d), −20.5(d)^b (CD$_2$Cl$_2$)	−78.84^a (CD$_2$Cl$_2$)	$^2J_{P–P}$ = 110^b	**3^{iPr}H**	−5.15^a (CD$_2$Cl$_2$)	−77.01^a (CD$_2$Cl$_2$)	
3^{iPr}	+28.37^a (CD$_2$Cl$_2$), +26.95^a (CD$_3$CN)	−78.84^a (CD$_2$Cl$_2$)		**3^{Ph} + LiBEt$_3$H**^{c}	−19.07, −19.82, −20.06^a (CDCl$_3$)	−78.35, −78.87^a (CDCl$_3$)	^{1}H NMR: 6.40(t) (J = 20.2, Ge–H$_2$)
3^{Ph}	−6.32^a (CDCl$_3$)	−79.74^a (CDCl$_3$)		**3^{iPr} + Et$_3$SiH**^{c,d}	+28.51 (**3^{iPr}**), +20.28 (P–H), +12.16 (P^{i}Pr$_2$)^a (CD$_2$Cl$_2$)		$^1J_{P–H}$ = 476
3^{iPr}OPEt$_3$^{c}	+73.4 (bound Et$_3$PO), −12.0 (P^{i}Pr$_2$)^a (CD$_2$Cl$_2$)			**3^{Ph} + Et$_3$SiH**^{c,e}	−19.0^a (CDCl$_3$)	−77.43^a (CDCl$_3$)	$^2J_{P–H}$ = 30.4
3^{Ph}OPEt$_3$^{c}	+71.59 (bound Et$_3$PO), −6.30 (**3^{Ph}**), −13.38 (PPh$_2$)^a (CDCl$_3$)			**3^{Ph} + aldehyde**^{c}	36.02–32.08, −19.26^a (CDCl$_3$)		

^{a} Chemical shift values at room temperature. ^{b} Chemical shift values at low temperature. ^{c} *In situ* NMR. ^{d} Measured after 2 days. ^{e} Measured after one day.

lithiated **L^{iPr}–Br** and GeCl$_4$ in a 2 : 1 ratio also led to the formation of **1^{iPr}**. An anion exchange reaction of **1^{iPr}** with one equivalent of trimethylsilyl trifluoromethane sulfonate (TMSOTf) followed by crystallization in DCM resulted in the isolation of **2^{iPr}** (Scheme 1a). **2^{iPr}** was characterized in the solution state using NMR spectroscopy displaying the characteristic ^{31}P{^{1}H} NMR chemical shift at −10.8 ppm.

The molecular structure[25] of **1^{iPr}** shows that the cationic part has an overall distorted trigonal bipyramidal (TBP) geometry with two pendant ^{i}Pr$_2$P groups occupying axial sites. Two Ge–C and one Ge–Cl bond constitute the trigonal plane with the sum of angles at the Ge atom close to 360°. The Ge1–P1 and Ge1–P2 bond lengths are 2.544(1) and 2.654(1) Å, respectively, which are longer than those of [GeF$_3$(Ph$_2$PCH$_2$CH$_2$PPh$_2$)(OTf)] (avg. Ge–P = 2.43 Å)[5] and diaminodiphosphine stabilized bis(chlorogermyliumylidene) (avg. Ge–P = 2.44–2.50 Å).[26] The structural parameters of the cationic part in **2^{iPr}** (Fig. 2a) are analogous to **1^{iPr}**. The triflate counter anion in **2^{iPr}** is located far away from the Ge cationic site (closest Ge–O contact being 5.7 Å).

The formation of **3^{iPr}** can either proceed as a one-pot reaction between **1^{iPr}** and two equivalents of TMSOTf in DCM or stepwise chloride abstraction from **1^{iPr}** via the intermediacy of **2^{iPr}** (Scheme 1a). Colourless crystals of **3^{iPr}** were obtained from the concentrated THF solution. The characteristic ^{31}P{^{1}H} NMR chemical shift values obtained for **3^{iPr}** in CD$_3$CN (+27.0 ppm) and CD$_2$Cl$_2$ (+28.4 ppm) are similar, which invalidates possible solvent coordination.

The solid-state structure of **3^{iPr}** (Fig. 3a) shows a spirocyclic geometry[19a] with the Ge atom at the nexus and having two non-coordinating triflate counter anions (closest Ge–O contact being
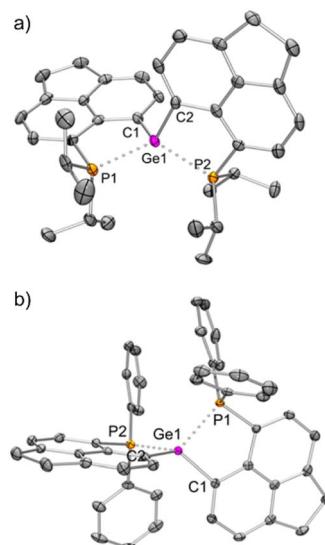

Fig. 3 Molecular structures of (a) **3^{iPr}** and (b) **3^{Ph}** (H atoms, solvent molecules and triflate anions have been removed for clarity; thermal ellipsoid 50%). Selected bond lengths [Å] and angles [°]: (a) Ge1–C1 = 1.923(5), Ge1–C2 = 1.923(5), Ge1–P1 = 2.350(1), Ge1–P2 = 2.363(1); C1–Ge1–C2 = 112.5(2), P1–Ge1–P2 = 122.4(1), C1–Ge1–P1 = 90.9(2), C2–Ge1–P2 = 91.4(2), C1–Ge1–P2 = 120.8(2), C2–Ge1–P1 = 121.2(2); (b) Ge1–C1 = 1.924(3), Ge1–C2 = 1.920(3), P1–Ge1 = 2.344(1), Ge1–P2 = 2.338(1); C2–Ge1–C1 = 126.8(1), C2–Ge1–P2 = 91.5(1), C1–Ge1–P2 = 116.1(1), C2–Ge1–P1 = 115.7(1), C1–Ge1–P1 = 91.2(1), P2–Ge1–P1 = 118.1(1).

5.8 Å). Due to the presence of dipositive charges in **3^{iPr}**, the Ge–C (avg. 1.92 Å) and Ge–P (avg. 2.36 Å) bond lengths are significantly shorter compared to those of **2^{iPr}**. The strongly electron-donating nature of the two intramolecular ^{i}Pr$_2$P groups adequately stabilizes the Ge(IV) di-cation in **3^{iPr}** in an overall tetra-coordinated environment.

In the case of the diphenylphosphanyl donor, the neutral compound [L$^{Ph}_2$GeCl$_2$] **1^{Ph}** could be obtained from the reaction between lithiated **L^{Ph}–Br** and GeCl$_4$ taken in a 2 : 1 ratio in a THF medium (Scheme 1b and Fig. S96, see the ESI† for Experimental procedures). Chloride abstractions from **1^{Ph}** using one and two equivalents of TMSOTf in DCM led to the formation of mono-cationic **2^{Ph}** and di-cationic **3^{Ph}** compounds, respectively (Scheme 1b). The characteristic peaks in ^{31}P{^{1}H} NMR spectra for **2^{Ph}** and **3^{Ph}** appear at −13.2 and −6.3 ppm respectively.

Unlike **2^{iPr}**, the molecular structure of **2^{Ph}** depicts a distorted tetrahedral geometry (Fig. 2b). Compared to **2^{iPr}**, the Ge1–P1 bond length has noticeably reduced in **2^{Ph}** (2.357(1) Å). Another Ge1···P2 bond distance in **2^{Ph}** is 3.012(1) Å. The triflate anion is far away from the Ge atom (closest Ge–O contact being 7.2 Å). The low temperature ^{31}P{^{1}H} NMR for **2^{Ph}** echoes the presence of two inequivalent phosphines exhibiting chemical shift values at −3.0 and −20.5 ppm.

The solid-state structure of **3^{Ph}** exhibits a spiro-geometry with similar bond parameters to those in **3^{iPr}** (Fig. 3b). There are two non-coordinated triflate anions (closest Ge–O contact being 4.2 Å) present in the asymmetric unit. Both **3^{iPr}** and **3^{Ph}** in

Fig. 2 (a) Molecular structures of (a) **2^{iPr}** and (b) **2^{Ph}** (H atoms, solvent molecule and triflate anion have been removed for clarity; thermal ellipsoid 50%). Selected bond lengths [Å] and angles [°]: (a) Ge1–Cl1 = 2.228(2), Ge1–C1 = 1.988(4), Ge1–P1 = 2.643(1); C1–Ge1–C1 = 147.9(2), Cl1–Ge1–C1 = 106.1(1), Cl1–Ge1–P1 = 86.9(1), P1–Ge1–P1 = 173.9(1); (b) Ge1–C1 = 1.922(3), Ge1–C2 = 1.926(3), Ge1–Cl1 = 2.215(1), Ge1–P1 = 2.357(1); C1–Ge1–C2 120.0(1), C1–Ge1–Cl1 = 104.8(1), C2–Ge1–Cl1 = 104.2(1), C1–Ge1–P1 = 91.1(1), C2–Ge1–P1 = 135.5(1), Cl1–Ge1–P1 = 96.4(1).

the solid-state show no sign of decomposition when exposed to air for a day.

The optimized geometries of $2o^{iPr}$, $2o^{Ph}$, $3o^{iPr}$ and $3o^{Ph}$ at the TPSS-D3(BJ)/def2-TZVPP level of theory are in close agreement with the X-ray parameters (see the ESI† for the detailed theoretical part). On par with the experimental findings, Natural Bond Orbital (NBO) analyses for $2o^{iPr}$ suggest significant donor–acceptor (D–A) interactions (avg. 125 kcal mol^{-1}) for $LP_{P1} \rightarrow LP^*_{Ge}$ and $LP_{P2} \rightarrow LP^*_{Ge}$. However, dissimilar bonding situations in $2o^{Ph}$ between Ge1–P1 (covalent) and Ge1–P2 (D–A interaction) were confirmed by NBO and AIM (Atoms in Molecules) analyses. The calculated Wiberg bond index (WBI) of Ge1–P2 in $2o^{Ph}$ possesses dative nature with a value of 0.183 (0.712 for Ge1–P1). Additionally, no bonding orbital for Ge1–P2 was observed from the NBO analyses. Instead, only one D–A interaction $(LP_{P2} \rightarrow LP^*_{Ge})$ is determined in $2o^{Ph}$ with a stabilization energy of 32 kcal mol^{-1}. Furthermore, we have performed AIM analyses. A negative Laplacian value at the BCPs (bond critical points) is associated with shared interactions, indicating covalent bonds, and positive Laplacian values reflect closed shell interactions such as ionic or dative bonds. In the case of $2o^{Ph}$, the higher positive $\nabla^2\rho(r)$ value on Ge–P2 shows dative bonding character.

The frontier molecular orbitals (FMOs) of $3o^{iPr}$ and $3o^{Ph}$ reflect similar contributions in terms of Ge–C and Ge–P σ^* orbitals (Fig. 4a and b). The orbital scenario is analogous to those observed in the catecholato phosphonium ion[19a] or stibonium salt.[27] There is no pure vacant p-orbital available[28] on the central Ge atom in both cases. WBI calculations predict the values of 0.804 ($3o^{iPr}$) and 0.770 ($3o^{Ph}$) for Ge–P bonds, displaying a mostly covalent bonding situation. The dispersion of positive charges among the P (+1.161, +1.145 for $3o^{iPr}$; +1.174, +1.174 for $3o^{Ph}$) and Ge (+1.136 for $3o^{iPr}$; +1.157 for $3o^{Ph}$) sites is evident from NBO partial charges and the electrostatic potential map analyses (Fig. 4c and d). Canonical forms describing the dispersion of positive charges in $3o^{iPr}$ and $3o^{Ph}$ (F) are depicted in Fig. 1.

Lewis acidic properties of Ge(IV) di-cationic compounds

We have studied the effective Lewis acidity of both 3^{iPr} and 3^{Ph} from induced ^{31}P NMR shift of triethylphosphine oxide (Et$_3$PO) in the Gutmann–Beckett (GB) method (see the ESI† for

Fig. 4 (a) Acceptor orbitals in $3o^{iPr}$; (b) LUMO in $3o^{Ph}$; electrostatic potential map for (c) $3o^{iPr}$ and (d) $3o^{Ph}$.

details).[29] Et$_3$PO adducts were targeted by employing varying equivalents of Et$_3$PO (0.2 to 3.0 equivalents) in deuterated solvents. The addition of 0.2 equivalents of Et$_3$PO to 3^{iPr} gave numerous peaks at +75.7, +74.2, −12.3 and −18.2 ppm. The complexity of the $^{31}P\{^1H\}$ NMR spectra obtained at room temperature impeded the Lewis acidity scaling of 3^{iPr} by the GB method. However, we have observed peaks appearing at +73.4 and −12.0 ppm in the $^{31}P\{^1H\}$ NMR spectrum, when a 1:1 mixture of 3^{iPr} and Et$_3$PO was prepared in CD$_2$Cl$_2$ at −78 °C and subsequently raised to room temperature. This gave an induced $^{31}P\{^1H\}$ NMR chemical shift of Et$_3$PO for 3^{iPr} ($\Delta^{31}P$ = 21.3 ppm) with respect to the free Et$_3$PO (δ for free Et$_3$PO in the same solvent is 52.1 ppm).

In the case of 3^{Ph}, we have noticed the induced $^{31}P\{^1H\}$ NMR chemical shift from the addition of 0.2 equivalents of Et$_3$PO in CDCl$_3$ ($\Delta^{31}P$ = 21.6 ppm, δ for free Et$_3$PO in the same solvent is 50.0 ppm); without any complexity observed in the NMR spectrum at room temperature. These $\Delta^{31}P$ values are close to the values reported for the Si(IV) di-cations ($\Delta^{31}P$ = 23.5 ppm for [Ph$_2$Si(terpy)]$^{2+}$).[7] Both 3^{iPr} and 3^{Ph} exhibit similar effective Lewis acidity as obtained following the GB method. The peak at +71.6 ppm in the $^{31}P\{^1H\}$ NMR spectrum assigned to the bound Et$_3$PO is shifted up-field upon increasing the amount of Et$_3$PO. This obvious shift is due to the expected weak acceptor ability upon further Et$_3$PO coordination at the cationic site.[10f] We have crystallized the mono-adduct $3^{Ph}OPEt_3$ (Fig. S97†) under low temperature conditions from the reaction between 3^{Ph} and Et$_3$PO. The molecular structure of $3^{Ph}OPEt_3$ shows a penta-coordinated Ge site. Interestingly, the solution-state NMR study of $3^{Ph}OPEt_3$ shows characteristic $^{31}P\{^1H\}$ NMR chemical shifts at +68.5 and −20.5 ppm along with a peak at −6.3 ppm assigned to the in situ generated free 3^{Ph}. This observation reflects the presence of the equilibrium in the solution-state.

Despite the dispersion of dipositive charges over the P–Ge–P sites in 3^{iPr} and 3^{Ph}, we have observed the preferential binding of Lewis bases such as Et$_3$PO and 4-N,N'-dimethylaminopyridine (DMAP) at the Ge site (Scheme 2). The reaction between 3^{iPr} and DMAP taken in a 1:1 ratio gave $3^{iPr}DMAP$, which was crystallized in small amounts from DCM/hexane layering at room temperature (Scheme 2). Single crystals of dimethylamino pyridium triflate were obtained in large amounts, which were separated from the $3^{iPr}DMAP$ crystals. The molecular structure of $3^{iPr}DMAP$ from X-ray analysis reveals an overall TBP geometry with the DMAP coordination at one of the trigonal planar equatorial sites of the Ge atom (Fig. S98†). However, $3^{iPr}DMAP$ is unstable under room temperature conditions in the solution state. The $^{31}P\{^1H\}$ NMR of in situ generated $3^{iPr}DMAP$ at −40 °C in CD$_2$Cl$_2$ shows a peak at −13.2 ppm in addition to the unco-ordinated 3^{iPr} peak (+28.4 ppm) present in the reaction medium. These peaks gradually disappeared upon warming to room temperature, ultimately giving new peaks at +75.7 ppm and −18.2 ppm (vide supra). We have observed a peak at +12.9 ppm in the ^1H NMR spectrum corresponding to the formation of the conjugate acid dimethylamino pyridium triflate. Similar side-reactions might be involved in the reaction between 3^{iPr} and donors (Et$_3$PO and DMAP), as was reported earlier by Stephan et al.[30]
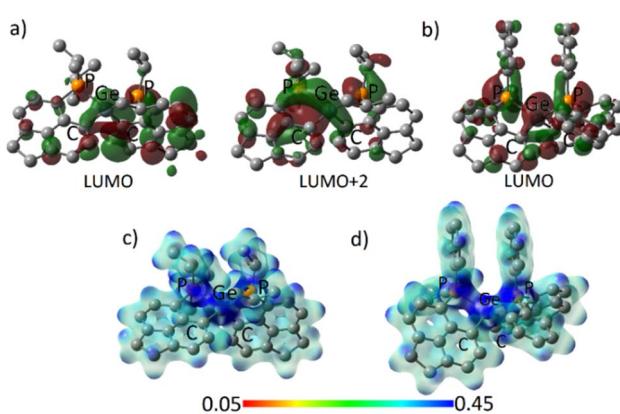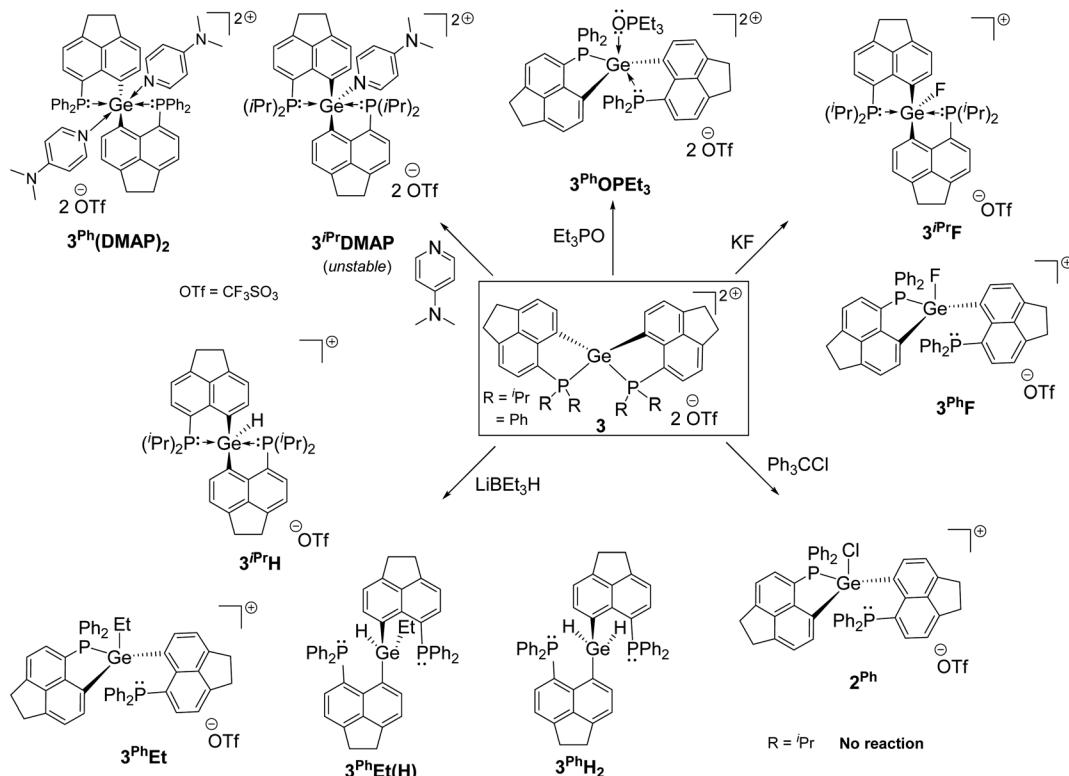
**Scheme 2** Anion/Lewis base binding and bond activation by the Ge(IV) di-cationic compounds (see the ESI† for detailed spectroscopic and experimental procedures of each reaction).

A dynamic process[13a] between mono- and bis-adduct formation was observed upon reacting 3^{Ph} with one equivalent of DMAP at room temperature. The NMR scale reaction in CDCl$_3$ shows a peak at −18.5 ppm and a broad peak centered at −27.0 ppm in the ^{31}P{^{1}H} NMR spectrum. The gradual decrease in temperature up to −50 °C resulted in a complete disappearance of the peak at −18.5 ppm. Concurrently two close sharp peaks at ∼−29 ppm appeared along with the generation of the peak for 3^{Ph} at −6.3 ppm. Inferring from this NMR study, a bis-adduct was isolated (corresponding peak at ∼−29 ppm) from the reaction between DMAP and 3^{Ph} at −35 °C. The crystallization from DCM/pentane layering at the same temperature gave single crystals of *trans* bis-adduct $3^{Ph}(DMAP)_2$ (Fig. S99†). As a matter of fact, in this case we find the spontaneous formation of the more favourable hexa-coordinated bis-adduct over the mono-adduct at lower temperatures.[11d] The octahedral coordination type at the Ge atom of $3^{Ph}(DMAP)_2$ comprises two L^{Ph} in the equatorial plane and two DMAPs occupying the axial sites. Thus, dynamic processes were observed for the adducts formed between 3^{Ph} and donors.

The preferential binding of donor groups at the Ge site is associated with the relief in constraint on going from a strained spiro-geometry in 3^{iPr} and 3^{Ph} to the relaxed TBP ($3^{iPr}DMAP$) and distorted tetrahedral geometry ($3^{Ph}OPEt_3$) in the adducts, respectively. Notably, this results in a handful of penta-coordinated Ge compounds obtained having TBP geometry which are uncommon in Ge chemistry.[11d] The viable expansion of the *peri*-distances[22] in the two intramolecular P–Ge bonds in

3^{iPr} and 3^{Ph} allows smooth structural rearrangements with the addition of nucleophiles.

We have validated the above understanding from the deformation energy[9,29] values obtained in the spiro- to TBP geometric transformation. We have prepared $3^{iPr}F$ from the addition of one equivalent of KF to 3^{iPr} (Scheme 2), which exhibits a distorted TBP geometry (Fig. 5a) like 2^{iPr} in the solid state. DFT calculations reveal that the fluoride ion binding to 3^{iPr} involves a low deformation energy (E_{def} = 126 kJ mol$^{−1}$), falling within the range reported in the literature.[10g,19a,29] $3^{iPr}F$ was characterised by NMR spectroscopy in the solution state showing a characteristic triplet at −141.0 ppm ($^2J_{F–P}$ = 185 Hz) in the ^{19}F{^{1}H} NMR spectrum and a corresponding doublet in the ^{31}P{^{1}H} NMR spectrum (−10.2 ppm).

Like 3^{iPr}, the addition of one equivalent of KF led to the formation of $3^{Ph}F$ (Scheme 2) showing similar characteristic peaks in NMR spectra (δ ^{19}F{^{1}H}: −150.3 ppm, triplet, and $^2J_{P–F}$ = 100 Hz; δ ^{31}P{^{1}H}: −17.5 ppm). The molecular structure of $3^{Ph}F$ (Fig. 5b) resembles that of 2^{Ph}. The low temperature ^{31}P{^{1}H} NMR spectrum reveals the presence of inequivalent phosphines in $3^{Ph}F$. In this case, the release of the structural constraint occurs on going from spirocyclic 3^{Ph} to the relaxed geometry in $3^{Ph}F$ involving a deformation energy value of 148 kJ mol$^{−1}$.[10g,19a,29]

The calculations on the gas-phase fluoride ion affinity (FIA)[31] at the Ge sites give very high values of 873 kJ mol$^{−1}$ and 859 kJ mol$^{−1}$ for 3^{iPr} and 3^{Ph} respectively (gas-phase FIA for reference SbF$_5$ is 497 kJmol$^{−1}$) (see the ESI† for details).
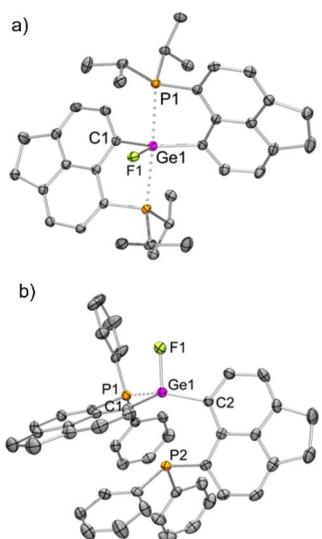
Fig. 5 Molecular structures of (a) $3^{iPr}F$ and (b) $3^{Ph}F$ (H atoms, solvent molecule and triflate anion have been removed for clarity; thermal ellipsoid 50%). Selected bond lengths [Å] and angles [°]: (a) Ge1–C1 = 1.951(2), Ge1–F1 = 1.785(2), Ge1–P1 = 2.565(1); C1–Ge1–C1 = 145.1(1), F1–Ge1–C1 = 107.5(1), P1–Ge1–P1 = 172.8(1), P1–Ge1–F1 = 86.4(1); (b) Ge1–F1 = 1.797(2), Ge1–C2 = 1.920(3), Ge1–C1 = 1.927(3), Ge1–P1 = 2.368(1), Ge1–P2 = 3.043(1); F1–Ge1–C2 = 102.1(1), F1–Ge1–C1 = 102.8(1), C2–Ge1–C1 = 120.6(1), F1–Ge1–P1 = 97.3(1), C2–Ge1–P1 = 137.3(1), C1–Ge1–P1 = 91.2(1).

However, the calculated FIA values in DCM solvated models decreased significantly giving the values of 194 kJ mol^{-1} and 190 kJ mol^{-1} for 3^{iPr} and 3^{Ph}, respectively (solvent corrected FIA for reference SbF$_5$ is 331 kJmol^{-1}). This is a common phenomenon observed due to solvation damping, being more pronounced with a cationic Lewis acid.[7,19a] Both 3^{iPr} and 3^{Ph} did not abstract the fluoride anion when reacted with [PPh$_4$][SbF$_6$] and hence are not Lewis superacids. The chloride ion affinity study using trityl chloride shows that only 3^{Ph} abstracts chloride with characteristic coloration[10g] and the NMR data reveal the formation of 2^{Ph} (Scheme 2 and Fig. S62, ESI†).

Gas-phase hydride ion affinity (HIA)[31] calculations also give very high values of 949 kJ mol^{-1} and 928 kJ mol^{-1} for 3^{iPr} and 3^{Ph}, respectively (gas-phase HIA for reference B(C$_6$F$_5$)$_3$ is 517 kJ mol^{-1}) (see the ESI† for details). Reasonable HIA values are obtained after considering the solvation in DCM: 254 kJ mol^{-1} and 269 kJ mol^{-1} for 3^{iPr} and 3^{Ph}, respectively (solvent corrected HIA for reference B(C$_6$F$_5$)$_3$ is 270 kJmol^{-1}). Thus, both 3^{iPr} and 3^{Ph} are hydrophilic in nature. 3^{iPr} efficiently abstracts the hydride from LiBEt$_3$H at room temperature leading to the formation of $3^{iPr}H$ (Scheme 2). The ^{1}H NMR spectrum of $3^{iPr}H$ reveals the Ge–H resonance as a triplet ($^2J_{P-H}$ = 36 Hz) at +7.2 ppm; the chemical shift value falls within the range of reported Ge-hydrides.[15] The molecular structure of $3^{iPr}H$ attains a distorted TBP geometry (Fig. S100†) analogous to 2^{iPr}. The Ge–H bond length of 1.540 Å in the optimized geometry $3o^{iPr}H$ agrees well with that found in the molecular structure of $3^{iPr}H$ (1.54(3) Å) (see the ESI† for details). The reaction of 3^{Ph} with two equivalents of LiBEt$_3$H gave the neutral $3^{Ph}H_2$ (Scheme 2). The

molecular structure of $3^{Ph}H_2$ is shown in Fig. S101.† The Ge⋯P distances in $3^{Ph}H_2$ are close to 3 Å; however they fall within the sum of van der Waal's radii ΣvdW(Ge–P) = 3.91 Å.[32] The ^{1}H NMR spectrum of $3^{Ph}H_2$ reveals a Ge–H$_2$ resonance at 6.4 ppm as a triplet (J_{P-H} = 20 Hz). The reaction between 3^{Ph} and one equivalent of LiBEt$_3$H followed by crystallization from different solvent combinations gives the single crystals of $3^{Ph}Et$ and $3^{Ph}H(Et)$ (Scheme 2 and Fig. S102, S103, ESI†), confirming B–C bond activation.[33] Thus, preliminary reactivity studies identify 3^{Ph} as a highly reactive di-cation.

Catalytic hydrosilylation of an aromatic aldehyde by the Ge(IV) di-cationic compounds

Given the hydrophilicity of the soft Ge-based Lewis acids 3^{iPr} and 3^{Ph}, we targeted the activation of the Si–H bond in Et$_3$SiH (see the ESI† for details).[34] Monitoring the reaction between 3^{iPr} and excess Et$_3$SiH at room temperature using ^{31}P NMR displays the formation of two new peaks at +20.3 ppm and +12.2 ppm along with retention of 3^{iPr}. The peak at +20.3 ppm showed a coupling of J_{PH} ≈ 476 Hz. Furthermore, ^{1}H–^{31}P 1D and 2D Heteronuclear Single Quantum Coherence (HSQC) NMR measurements (CNST2 optimized at 480 Hz) confirm that $^1J_{PH}$ = 476 Hz.[35] Thus, the Si–H bond activation and hydride binding occur preferentially at the P-site over the Ge-site giving $3^{iPr}–PH$. This is in contrast to $3^{iPr}H$ formed by hydride abstraction from LiBEt$_3$H (vide supra). Notably, although Si–H bond activation occurs at the P-site of 3^{iPr}, standing of the reaction mixture for 14 days ultimately led to Ge–H bond formation (t, $^2J_{P-H}$ = 36 Hz at +7.2 ppm) giving $3^{iPr}H$.

In contrast, 3^{Ph} activates the Si–H bond in Et$_3$SiH giving $3^{Ph}H$ (Scheme 3a) as the product within 24 hours (see the ESI† for details). However, the time dependent ^{31}P NMR monitoring of the initial reaction mixture displays a minor peak at +10.0 ppm with a coupling of $^1J_{PH}$ = 534 Hz corresponding to the P–H formation, which subsequently disappeared giving $3^{Ph}H$ within 24 hours. The ^{1}H NMR spectrum of $3^{Ph}H$ discloses the Ge–H resonance at +7.0 ppm as a triplet ($^2J_{P-H}$ = 30 Hz) and a corresponding doublet at −19.0 ppm in the ^{31}P{^{1}H} NMR spectrum. The ^{29}Si{^{1}H} NMR of the reaction mixture shows the corresponding formation of Et$_3$SiOTf (δ = +45.0 ppm).
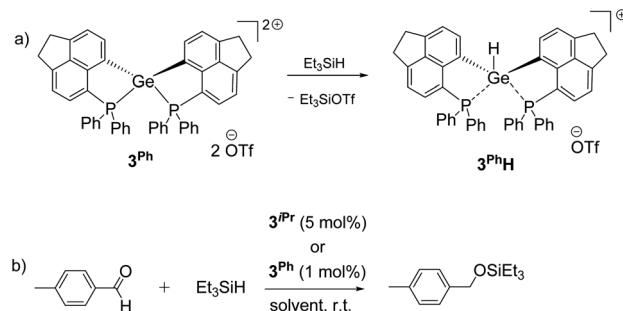
Scheme 3 (a) Si–H bond activation by 3^{Ph} leading to $3^{Ph}H$ within 24 hours; (b) hydrosilylation of p-methyl benzaldehyde using 3^{iPr} or 3^{Ph} as the catalyst (see the ESI† for the detailed spectroscopic and experimental procedures of each reaction).
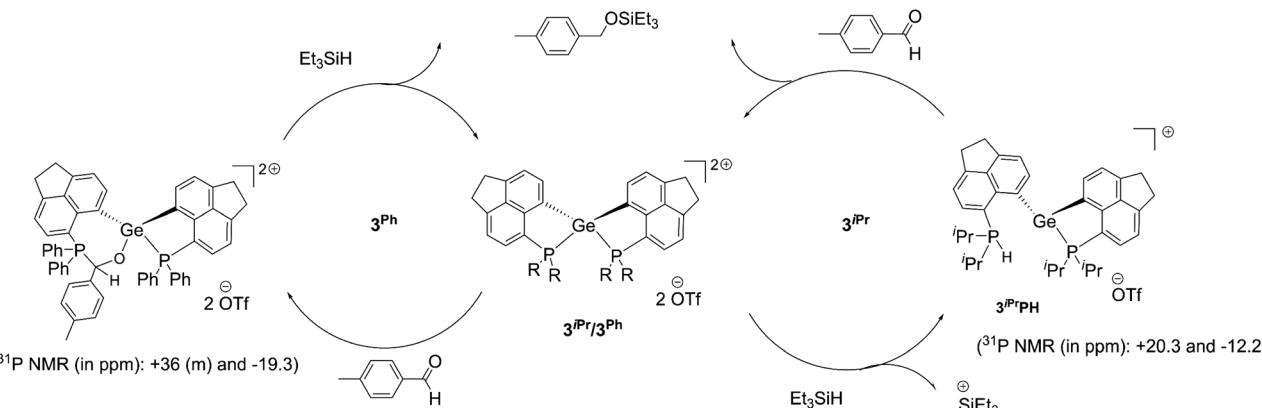
Scheme 4 Proposed catalytic cycle for the hydrosilylation of aromatic aldehydes using 3^{iPr} and 3^{Ph} as catalysts.

The above-mentioned observations suggest that the hydride binding initially occurs at the P-site due to the dispersion of dipositive charges over P–Ge–P units in these di-cationic species. Computational investigations done on the hydride migration from P to Ge for both 3^{iPr} and 3^{Ph} reveal the involvement of a relatively higher transition state energy barrier in the case of the former (Fig. S112, ESI†). The hydride migration mechanism proposed based on the DFT calculations performed on the cationic part of the compounds proves only the trends of the hydride shifts from P to Ge. Nonetheless, the very low energy barriers obtained are inadequate to support the longer time requirements for hydride migrations observed experimentally. Probably, the inclusions of the solvent models and counter anions to the systems would be able to resolve the disagreement at an associated extremely high computational cost. Thus, the hydride migration mechanism proposed herein is rather based on the experimentally observed data. Additionally, the strong electron donating nature of $^{i}Pr_2P$ compared to Ph_2P pushes electron density towards the Ge-site in 3^{iPr} thereby making the P-site appropriate for hydride. The ultimate formation of $3^{iPr}H$ or $3^{Ph}H$ stems from the geometric constraint empowered Lewis acidity at the Ge site of 3^{iPr} or 3^{Ph} respectively (*vide supra*).

Despite the differences observed in the reaction with Et_3SiH, the intrinsic hydrophilicity of 3^{iPr} and 3^{Ph} prompted us to perform a test reaction on the catalytic hydrosilylation[36] of *p*-methyl benzaldehyde with Et_3SiH at room temperature (Scheme 3b, see the ESI† for details). Using 5 mol% of 3^{iPr} led to the complete conversion to the silyl ether within 24 hours. It is observed from the ^1H NMR study that the aldehyde does not bind to the catalyst, unlike most Lewis acid catalysts.[10e] Thus, the reaction is likely to proceed *via* silane activation by 3^{iPr} (Scheme 4).[37] The NMR investigations of the catalytic reaction mixture show P-mediated Si–H bond activation (^1H NMR = +8.5 ppm; ^{31}P NMR = +20.2 ppm). The $^{29}Si\{^1H\}$ NMR spectrum shows the formation of a hydrosilylated product and the presence of Et_3SiH with the corresponding peaks at +8.9 ppm and +0.3 ppm, respectively. The $^{29}Si\{^1H\}$ NMR spectrum did not show the presence of Et_3SiOTf which is a competent catalyst. Nonetheless, the latter's presence in trace amounts and participation in the catalytic cycle cannot be completely neglected. The control experiment shows no hydrosilylated

product being formed, as confirmed from the ^1H NMR study of the reaction mixture containing *p*-methyl benzaldehyde and Et_3SiH (Fig. S94, ESI†).

Full conversion of *p*-methyl benzaldehyde to the silyl ether was achieved within 24 hours under room temperature conditions by using a lower catalyst loading to 1 mol% of 3^{Ph} (see the ESI† for details). Importantly, the aldehyde (in the absence of any other reactant) binds to 3^{Ph} as evident from the NMR study. The $^{31}P\{^1H\}$ NMR spectrum depicts a peak at −19.3 ppm and multiple peaks at around +36 ppm in addition to the peak for free 3^{Ph} (−6.3 ppm). Correspondingly, we have obtained single crystals from a THF solution of 3^{Ph} and excess aldehyde. The crystal structure shows the insertion of an aldehyde into the P–Ge bond in 3^{Ph} (Fig. S104, ESI†). Thus, a masked frustrated Lewis pair (FLP) type behavior[21,38] of 3^{Ph} was observed, which is unsurprising due to the adaptability of the P–Ge bond in *peri*-systems. The NMR spectrum recorded immediately after the addition of 3^{Ph} to the reaction mixture of the aldehyde and Et_3SiH also displays similar chemical shift values (−19.3 and around +36 ppm in the $^{31}P\{^1H\}$ NMR study). The NMR study did not show any peak arising from Si–H bond activation by 3^{Ph}. This suggests the formation of the carbonyl-FLP insertion product taking place at the initial stage of the catalytic cycle. Notably, no Et_3SiOTf formation is detected from the $^{29}Si\{^1H\}$ NMR monitoring (Fig. S93, ESI†). Thus, the catalytic hydrosilylation is likely to proceed *via* the carbonyl insertion followed by the R_3Si–H addition across the carbonyl functional group (Scheme 4). The catalyst 3^{Ph} is clearly observed after complete consumption of the reactants.

Thus, both 3^{iPr} and 3^{Ph} show different pathways catalysing the hydrosilylation of the aldehyde. Based on our experimental findings, while the former proceeds through the Si–H bond activation at the Lewis acidic site, the latter utilizes the masked FLP for the aldehyde insertion followed by Et_3Si–H addition to the C=O bond.

Conclusion

In this study, we have established the first examples of tetra-coordinated Ge(IV) di-cationic compounds 3^{iPr} and 3^{Ph}. This was achieved through the intramolecular stabilization of the Ge di-cationic site using a phosphine donor in *peri*-substituted

acenaphthene. The strong P–Ge bonds led to the dispersion of di-cationic charges over Ge and P sites. The simple anion binding or Lewis base coordination occurs exclusively at the Ge site owing to the release of the geometric constraint on going from the spiro-geometry of the di-cation to the distorted TBP/ tetrahedral geometry of the resultant species. Although the Si–H bond activation occurs initially at the P site for both the di-cationic species due to their dispersed di-positive charges, the migration of hydrides to the Ge site occurs promptly in the case of 3^{Ph} compared to 3^{iPr}. Preliminary tests on the catalytic hydrosilylation of the benzaldehyde demonstrate the involvement of two different catalytic pathways for the two catalysts 3^{iPr} and 3^{Ph}. In the case of 3^{iPr}, the catalytic hydrosilylation was initiated with Et3Si–H bond activation. On the other hand, masked Frustrated Lewis Pair (FLP) type reactivity led to hydrosilylated product formation for 3^{Ph} as the catalyst. Fine tuning the donor group properties in such charged *peri* species is being explored in our group for their applicability as catalysts in diverse organic transformations.

Data availability

All data associated with this publication are provided in the ESI.†

Author contributions

Investigation, methodology and formal analysis: Balakrishna Peddi and Souvik Khan. X-ray crystallography: Rajesh G. Gonnade. Computational study, comment and editing draft: Cem B. Yildiz. Conceptualization, funding acquisition, supervision, and writing-original draft: Moumita Majumdar.

Conflicts of interest

There are no conflicts to declare.

Acknowledgements

References

1 Selected references:(*a*) P. A. Rupar, V. N. Staroverov, P. J. Ragogna and K. M. Baines, *J. Am. Chem. Soc.*, 2007, **129**, 15138; (*b*) P. A. Rupar, V. N. Staroverov and K. M. Baines, *Science*, 2008, **322**, 1360; (*c*) Y. Xiong, T. Szilvási, S. Yao, G. Tan and M. Driess, *J. Am. Chem. Soc.*, 2014, **136**, 11300; (*d*) P. A. Rupar, R. Bandyopadhyay, B. F. T. Cooper, M. R. Stinchcombe, P. J. Ragogna, C. L. B. Macdonald and K. M. Baines, *Angew. Chem., Int. Ed.*, 2009, **48**, 5155; (*e*) F. Cheng, A. L. Hector, W. Levason, G. Reid, M. Webster and W. Zhang, *Angew. Chem., Int. Ed.*, 2009, **48**, 5152; (*f*) T. A. Engesser, M. R. Lichtenthaler, M. Schleep and I. Krossing, *Chem. Soc. Rev.*, 2016, **45**, 789; (*g*) V. S. V. S. N. Swamy, S. Pal, S. Khan and S. S. Sen, *Dalton Trans.*, 2015, **44**, 12903; (*h*) S. Biswas, N. Patel, R. Deb and M. Majumdar, *Chem. Rec.*, 2022, **22**, e202200003.

2 R. Bandyopadhyay, J. H. Nguyen, A. Swidan and C. L. B. Macdonald, *Angew. Chem., Int. Ed.*, 2013, **52**, 3469.

3 R. K. Raut and M. Majumdar, *Chem. Commun.*, 2017, **53**, 1467.

4 R. Suter, A. Swidan, C. L. B. Macdonald and N. Burford, *Chem. Commun.*, 2018, **54**, 4140.

5 R. P. King, W. Levason and G. Reid, *Dalton Trans.*, 2021, **50**, 17751.

6 A. P. M. Robertson, J. N. Fiedmann, H. A. Jenkins and N. Burford, *Chem. Commun.*, 2014, **50**, 7979.

7 A. Hermannsdorfer and M. Driess, *Angew. Chem., Int. Ed.*, 2020, **59**, 23132.

8 A. Hermannsdorfer and M. Driess, *Angew. Chem., Int. Ed.*, 2021, **60**, 13656.

9 (*a*) L. Greb, *Chem.–Eur. J.*, 2018, **24**, 17881; (*b*) L. O. Müller, D. Himmel, J. Stauffer, G. Steinfeld, J. Slattery, G. Santiso-Quiñones, V. Brecht and I. Krossing, *Angew. Chem., Int. Ed.*, 2008, **47**, 7659; (*c*) T. Thorwart and L. Greb, Lewis Superacids, in *Encyclopedia of Inorganic and Bioinorganic Chemistry*, 2021, DOI: 10.1002/9781119951438.eibc2758.

10 (*a*) H. F. T. Klare and M. Oestreich, *Dalton Trans.*, 2010, **39**, 9176; (*b*) H. F. T. Klare, L. Albers, L. Süsse, S. Keess, T. Müller and M. Oestreich, *Chem. Rev.*, 2021, **121**, 5889; (*c*) T. Müller, in *Functional Molecular Silicon Compounds I*, ed. D. Scheschkewitz, Structure and Bonding, Springer, 2013, ch. 3; (*d*) T. Stahl, H. F. T. Klare and M. Oestreich, *ACS Catal.*, 2013, **3**, 1578; (*e*) A. L. L. Martin, R. G. Bergman and T. D. Tilley, *J. Am. Chem. Soc.*, 2015, **137**, 5328; (*f*) R. Maskey, M. Schadler, C. Legler and L. Greb, *Angew. Chem., Int. Ed.*, 2018, **57**, 1717; (*g*) D. Hartmann, M. Schädler and L. Greb, *Chem. Sci.*, 2019, **10**, 7379; (*h*) F. S. Tschernuth, T. Thorwart, L. Greb, F. Hanusch and S. Inoue, *Angew. Chem., Int. Ed.*, 2021, **60**, 25799.

11 (*a*) H. C. Clark and C. J. Willis, *J. Am. Chem. Soc.*, 1962, **84**, 898; (*b*) D. P. Graddon and B. A. Rana, *J. Organomet. Chem.*, 1979, **165**, 157; (*c*) D. J. Brauer, H. Bürger and R. Eujen, *Angew Chem. Int. Ed. Engl.*, 1980, **19**, 836; (*d*) S. E. Denmark, R. T. Jacobs, G. Dai-Ho and S. Wilson, *Organometallics*, 1990, **9**, 3015; (*e*) S. Pelzer, B. Neumann, H.-G. Stammler, N. Ignat'ev and B. Hoge, *Chem.–Eur. J.*, 2016, **22**, 3327; (*f*) S. Pelzer, B. Neumann, H.-G. Stammler, N. Ignat'ev and B. Hoge, *Chem.–Eur. J.*, 2016, **22**, 16460; (*g*) T. A. Kinder, R. Pior, S. Blomeyer, B. Neumann,

H.-G. Stammler and N. W. Mitzel, *Chem.–Eur. J.*, 2019, **25**, 5899.

12 D. Roth, H. Wadepohl and L. Greb, *Angew. Chem., Int. Ed.*, 2020, **59**, 20930.

13 (*a*) A. T. Henry, T. P. L. Cosby, P. D. Boyle and K. M. Baines, *Dalton Trans.*, 2021, **50**, 15906; (*b*) D. Basu and H. P. Nayek, *Dalton Trans.*, 2022, **51**, 10587.

14 H. Fang, H. Jing, A. Zhang, H. Ge, Z. Yao, P. J. Brothers and X. Fu, *J. Am. Chem. Soc.*, 2016, **138**, 7705.

15 P. M. Keil and T. J. Hadlington, *Angew. Chem., Int. Ed.*, 2022, **61**, e202114143.

16 M. Karimi, E. S. Tabei, R. Fayad, M. R. Saber, E. O. Danilov, C. Jones, F. N. Castellano and F. P. Gabbai, *Angew. Chem., Int. Ed.*, 2021, **60**, 22352.

17 Selected reviews on Group 13 Lewis acids:(*a*) E. I. Davydova, T. N. Sevastianova and A. Y. Timoshkin, *Coord. Chem. Rev.*, 2015, **297**, 91; (*b*) I. B. Sivaev and V. I. Bregadze, *Coord. Chem. Rev.*, 2014, **270–271**, 75; Selected reviews on Group 14 Lewis acids: (*c*) H. Yamamoto, *Silicon(IV) Lewis Acids*, Wiley-VCH, Weinheim, 2000; (*d*) T. Müller, *Adv. Organomet. Chem.*, 2005, **53**, 155; (*e*) S. A. Weicker and D. W. Stephan, *Bull. Chem. Soc. Jpn.*, 2015, **88**, 1003; (*f*) D. J. Scott, N. A. Phillips, J. S. Sapsford, A. C. Deacy, M. J. Fuchter and A. E. Ashley, *Angew. Chem.*, 2016, **128**, 14958; Selected reviews on Group 15 Lewis acids: (*g*) C. B. Caputo, L. J. Hounjet, R. Dobrovetsky and D. W. Stephan, *Science*, 2013, **341**, 1374; (*h*) J. M. Bayne and D. W. Stephan, *Chem. Soc. Rev.*, 2016, **45**, 765; (*i*) D. W. Stephan, *Angew. Chem., Int. Ed.*, 2017, **56**, 5984; (*j*) J. M. Bayne and D. W. Stephan, *Chem.–Eur. J.*, 2019, **25**, 9350; (*k*) C. Lichtenberg, *Chem. Commun.*, 2021, **57**, 4483; (*l*) M. Yang, D. Tofan, C.-H. Chen, K. M. Jack and F. P. Gabbai, *Angew. Chem., Int. Ed.*, 2018, **57**, 13868.

18 (*a*) K. Chulsky, I. Malahov, D. Bawari and R. Dobrovetsky, *J. Am. Chem. Soc.*, 2023, **145**, 3786; (*b*) S. Volodarsky, D. Bawari and R. Dobrovetsky, *Angew. Chem., Int. Ed.*, 2022, **61**, e202208401; (*c*) A. Ben Saida, A. Chardon, A. Osi, N. Tumanov, J. Wouters, A. I. Adjieufack, B. Champagne and G. Berionni, *Angew. Chem., Int. Ed.*, 2019, **58**, 16889; (*d*) J. C. Gilhula and A. T. Radosevich, *Chem. Sci.*, 2019, **10**, 7177; (*e*) K. M. Marczenko, J. A. Zurakowski, M. B. Kindervater, S. Jee, T. Hynes, N. Roberts, S. Park, U. Werner-Zwanziger, M. Lumsden, D. N. Langelaan and S. S. Chitnis, *Chem.–Eur. J.*, 2019, **25**, 16414.

19 (*a*) D. Roth, J. Stirn, D. W. Stephan and L. Greb, *J. Am. Chem. Soc.*, 2021, **143**, 15845; (*b*) F. Ebner, L. M. Sigmund and L. Greb, *Angew. Chem., Int. Ed.*, 2020, **59**, 17118.

20 (*a*) D. W. Stephan, *J. Am. Chem. Soc.*, 2015, **137**, 10018; (*b*) D. W. Stephan, *Science*, 2016, **354**, aaf7229; (*c*) D. W. Stephan, *Chemistry*, 2020, **6**, 1520; (*d*) D. W. Stephan and G. Erker, *Angew. Chem., Int. Ed.*, 2010, **49**, 46; (*e*) D. J. Scott, M. J. Fuchter and A. E. Ashley, *Chem. Soc. Rev.*, 2017, **46**, 5689.

21 (*a*) D. Hartmann, S. Braner and L. Greb, *Chem. Commun.*, 2021, **57**, 8572; (*b*) I. Mallov, A. J. Ruddy, H. Zhu, S. Grimme and D. W. Stephan, *Chem.–Eur. J.*, 2017, **23**,

17692; (*c*) T. Thorwart, D. Hartmann and L. Greb, *Chem.–Eur. J.*, 2022, **28**, e202202273; (*d*) S. Freitag, J. Henning, H. Schubert and L. Wesemann, *Angew. Chem., Int. Ed.*, 2013, **52**, 5640; (*e*) J. Schneider, K. M. Krebs, S. Freitag, K. Eichele, H. Schubert and L. Wesemann, *Chem.–Eur. J.*, 2016, **22**, 9812; (*f*) J. Schneider, C. P. Sindlinger, S. M. Freitag, H. Schebert and L. Wesemann, *Angew. Chem., Int. Ed.*, 2017, **56**, 333.

22 (*a*) E. Hupf, E. Lork, S. Mebs and J. Beckmann, *Organometallics*, 2014, **33**, 2409; (*b*) J. Beckmann, E. Hupf, E. Lork and S. Mebs, *Inorg. Chem.*, 2013, **52**, 11881; (*c*) P. Kilian, F. R. Knight and J. D. Woollins, *Chem.–Eur. J.*, 2011, **17**, 2302; (*d*) Y. V. Vishnevskiy, A. A. Otlyotov, J.-H. Lamm, H.-G. Stammler, G. V. Girichev and N. W. Mitzel, *Phys. Chem. Chem. Phys.*, 2023, **25**, 11464.

23 (*a*) V. Kumar, R. G. Gonnade, C. B. Yildiz and M. Majumdar, *Angew. Chem., Int. Ed.*, 2021, **60**, 25522; (*b*) S. S. Chitnis, A. P. Robertson, N. Burford, J. J. Weigand and R. Fischer, *Chem. Sci.*, 2015, **6**, 2559.

24 N. C. Gonnella, C. Busacca, S. Campbell, M. Eriksson, N. Grinberg, T. Bartholomeyzik, S. Ma and D. L. Norwood, *Magn. Reson. Chem.*, 2009, **47**, 461.

25 CCDC numbers: 2223776 (**1^{iPr}**), 2223777 (**2^{iPr}**), 2223780–2223782 (**3^{iPr}**, **3^{iPr}H**, **3^{iPr}F**), 2223784 (**3^{iPr}DMAP**), 2256454–2256458 (**1^{Ph}**, **2^{Ph}**, **3^{Ph}**, **3^{Ph}(DMAP)_2**, **3^{Ph}Et_3PO**), 2256463 (**3^{Ph}F**), 2256466–2256468 (**3^{Ph}H_2**, **3^{Ph}Et**, **3^{Ph}H(Et)**), 2256567 (**3^{Ph}Oald**).

26 P. Sahoo, R. K. Raut, D. Maurya, V. Kumar, P. Rani, R. G. Gonnade and M. Majumdar, *Dalton Trans.*, 2019, **48**, 7344.

27 B. Pan and F. P. Gabbai, *J. Am. Chem. Soc.*, 2014, **136**, 9564.

28 F. Ebner, H. Wadepohl and L. Greb, *J. Am. Chem. Soc.*, 2019, **141**, 18009.

29 P. Erdmann and L. Greb, *Angew. Chem., Int. Ed.*, 2022, **61**, e202114550.

30 M. H. Holthausen, R. R. Hiranandani and D. W. Stephan, *Chem. Sci.*, 2015, **6**, 2016.

31 (*a*) P. Erdmann, J. Leitner, J. Schwarz and L. Greb, *ChemPhysChem*, 2020, **21**, 987; (*b*) P. Erdmann and L. Greb, *ChemPhysChem*, 2021, **22**, 935.

32 A. Bondi, *J. Phys. Chem.*, 1964, **68**, 441.

33 D. Carmichael, P. L. Floch, H. G. Trauner and F. Matthey, *Chem. Commun.*, 1996, 971.

34 (*a*) G. I. Nikonov, S. F. Vyboishchikov and O. G. Shirobokov, *J. Am. Chem. Soc.*, 2012, **134**, 5488; (*b*) A. Y. Houghton, J. Hurmalainen, A. Mansikkamäki, W. E. Piers and H. M. Tuononen, *Nat. Chem.*, 2014, **6**, 983.

35 M. H. Holthausen, J. M. Bayne, I. Mallov, R. Dobrovetsky and D. W. Stephan, *J. Am. Chem. Soc.*, 2015, **137**, 7298.

36 (*a*) D. J. Parks and W. E. Piers, *J. Am. Chem. Soc.*, 1996, **118**, 9440; (*b*) W. E. Piers and T. Chivers, *Chem. Soc. Rev.*, 1997, **26**, 345.

37 D. J. Parks, J. M. Blackwell and W. E. Piers, *J. Org. Chem.*, 2000, **65**, 3090.

38 A. Dajnak, E. Maerten, N. Saffon-Merceron, A. Baceiredo and T. Kato, *Organometallics*, 2020, **39**, 3403.